LAWRENCE
LIVERMORE
NATIONAL
LABORATORY

LLNL-JRNL-404468

# The Magnetic Field Structure of a Snowflake Divertor

D. D. Ryutov, R. H. Cohen, T. D. Rognlien, M. V. Umansky

June 5, 2008

Physics of Plasmas

## Disclaimer

# The magnetic field structure of a snowflake divertor

D.D. Ryutov, R.H. Cohen, T.D. Rognlien, M.V. Umansky

Lawrence Livermore National Laboratory, 94551, Livermore, CA

**Abstract**

The snowflake divertor exploits a tokamak geometry in which the poloidal magnetic field null approaches second order; the name stems from the characteristic hexagonal, snowflake-like, shape of the separatrix for an exact second-order null. The proximity of the poloidal field structure to that of a second-order null substantially modifies edge magnetic properties compared to the standard X-point geometry; this, in turn, affects the edge plasma behavior. Modifications include: 1) The flux expansion near the null-point becomes 2-3 times larger. 2) The connection length between the equatorial plane and divertor plate significantly increases. 3) Magnetic shear just inside the separatrix becomes much larger. 4) In the open-field-line region, the squeezing of the flux-tubes near the null-point increases, thereby causing stronger decoupling of the plasma turbulence in the divertor legs and in the main SOL. These effects can be used to reduce the power load on the divertor plates and/or to suppress the "bursty" component of the heat flux. It is emphasized that the snowflake divertor can be created by a relatively simple set of poloidal field coils situated beyond the toroidal field coils. Analysis of the robustness of the proposed divertor configuration with respect to changes of the plasma current distribution is presented and it is concluded that, even if the null is close to the second order, the configuration is quite robust.

## I. INTRODUCTION

Fusion reactors based on tokamaks will have to deal with very high heat loads on the divertor plates (e.g., Ref. [1, 2]). Reducing these loads would significantly broaden parameter space for these systems and improve economic characteristics of reactors.

In recent years, several approaches to solving this problem have been considered. Some are based on the use of coatings of the inner walls by material with small recycling coefficient (in particular lithium, see Refs. 3, 4). Other are based on a change of canonical geometry of the X-point divertor (e.g., [1, 5-8]), yet other pursue an active control over plasma turbulence, especially in the divertor legs [9, 10]. In principle, combinations of any of the two or of all three approaches can be envisaged. Eventual choice will be made based on a variety of considerations, including details of plasma equilibrium, life-time and maintainability of in-vessel components, the complexity of the magnetic system, and many other. The decision can be made only on the basis of an integrated design which is still far away in future. So, parallel pursuit of several approaches seems quite reasonable now.

In this paper we consider some details of the divertor configuration described in Ref. [6] and called there a "snowflake" divertor. This divertor exploits a tokamak geometry in which the poloidal magnetic field null approaches second order; the name stems from the characteristic hexagonal, snowflake-like, shape of the separatrix for an

exact second-order null (Fig. 1). The poloidal magnetic field in this latter case is a quadratic function of the distance to null, whereas in the standard X-point configuration it is a linear function. This means that a flux expansion is much larger in the vicinity of a null of a snowflake divertor, and one can try to exploit this fact for reducing the divertor heat load.

When using the terms "X-point divertor" or "standard X-point configuration", we mean a configuration with an X-shaped separatrix near the null point. This should not be confused with a recently proposed "X – divertor," where additional coils cause significant reduction of the magnetic field in the divertor legs at some distance from the X-point [1, 5], and even more recent "super-X divertor" [8], where further reduction of the heat load is expected to occur due to a significant increase the major radius of strike points.

To make the magnetic geometry of the snowflake robust enough with respect to possible uncontrollable variations of the plasma current, it was suggested to use a "snowflake-plus" mode [5], where the divertor current would be a few percent higher than the one that corresponds to an exact second-order null. In such a case, in a small area around the null-point, the magnetic field strength varies linearly with the distance, but very soon the quadratic dependence takes over and all the potential advantages of the snowflake geometry remain intact. There is an option of operating at the divertor current below the optimum value. This leads to formation of a "snowflake-minus" configuration [5], where there appear two closely situated X-points on the separatrix. Although this configuration is also of significant interest, it has a line (not point) contact of the private flux region and the core plasma, which brings too many new features to the picture. We leave the analysis of the snowflke-minus configuration for future work and concentrate here on snowflake and snowflake-plus configurations.

Some initial characterization of the magnetic geometry of the snowflake configuration and its topological stability has been done in Refs. [6, 7]. There are, however, several important characteristics of the snowflake geometry which had not been discussed in Refs. [6, 7] and which will be described in this paper. First, in the snowflake geometry, the magnetic shear just *inside* the separatrix strongly increases compared to the standard X-point configuration. Second, the squeezing of fluxtubes passing near the null-point *outside* the separatrix (see discussion of this effect in Ref. [11]) also becomes stronger. It is important to know the magnitude of both effects as they serve as input into analysis of bursty plasma behavior on the tokamak edge. In particular, the internal shear is an input parameter for the analysis of edge instabilities leading to development of Edge Localized Modes (ELM), e.g., [12, 13], whereas the squeezing of the external fluxtube is an input parameter for the evaluation of the velocity of blobs (e.g., [14, 15]).

Other characteristics include the flux expansion dependence on the distance from the separatrix and the connection length between the equatorial plane and the divertor plate. The latter two parameters are input parameters for the assessment of the problem of plasma detachment and design of radiative divertors (e.g., [1, 2, 16]).

As we will see, the largest contribution to all these parameters comes from the vicinity of the null-point. Therefore, significant progress in evaluating them can be made on the basis of the magnetic field expansions near the null point. Accordingly, we present these expansions in the next section (Sec. II). Sec. III relates the flux surfaces near the null to their position in the equatorial plane. Sec. IV covers the flux expansion. Sec. V is

concerned with the connection length. Sec. VI describes safety factor q and magnetic shear just inside the separatrix. Sec. VII deals with the flux tube mapping in the open field lines region. Sec. VIII is concerned with the reaction of the divertor field structure to possible uncontrollable variations of the plasma current. Finally, Sec. IX contains summary and discussion. Some more lengthy calculations are performed in Appendices A and B.

We present results in an easy-to-use form, without attempting bring them beyond most significant terms. A complete characterization of the magnetic geometry requires analysis of the global equilibrium, but this would already be a task specific for particular devices and would go well beyond the scope of this paper.

## II. GENERAL GEOMETRY AND APPROPRIATE EXPANSIONS

The second-order null of the poloidal field, in place of a standard first-order null, can be introduced in such a way that the overall plasma configuration would not change significantly, aside from the changes occurring in the vicinity of the null point. Some of the examples of such a behavior are given in Refs. [6, 7]. This is one of the signs of flexibility of the snowflake configuration. The fact that the field structure changes only in the vicinity of the null-point, allows one to rely on the expansions of the poloidal field near the null point. The general procedures for such expansions have been described in Refs. [6, 7]. Here we just mention that, in order to properly describe the snow-flake configuration, on has to expand the flux function to the third order in the distance from the null-point.

In the immediate vicinity of the null point one can neglect the toroidicity effects and consider a planar structure of the poloidal field. We will use Cartesian coordinates, $x$ and $z$, in the poloidal plane; the origin will be in the null-point. We introduce poloidal flux function $\Phi(x,z)$ so that

$$B_x = -\frac{\partial \Phi}{\partial z}; \quad B_z = \frac{\partial \Phi}{\partial x} \tag{1}$$

We start from the situation where the null is exact second order, and where the expansion of the flux function starts from the cubic terms. The separatrix near the null-point has then a characteristic hexapole shape (Fig. 1). We will orient the Cartesian coordinate frame so that the axis $z$ is directed from the null-point to the core plasma and lies in the symmetry plane, and axis $x$ directed perpendicularly. Note that we use notation ($x$, $z$), not ($x$, $y$) for the coordinates in the poloidal plane; this is a standard notation in the papers dealing with shaped plasmas. The expansion in this frame has a form [6]:

$$\Phi = A\frac{I}{c}\left(x^2 z - \frac{z^3}{3}\right), \tag{2}$$

where $I$ is the plasma current, $c$ is speed of light, and the parameter $A$ of the dimension of the inverse cube of the length characterizes the scale at which the poloidal magnetic field varies near the null point. The CGS system of units is used throughout this paper.

As a reference system, we often use a simple magnetic field configuration created by 3 wires , Fig. 1. For this configuration

$$A = \frac{a+b}{a^2 b^2}, \tag{3}$$

where dimensions are shown in Fig. 1.

In Ref. 1 it was pointed out that exact snowflake configuration is topologically unstable, and that it might be beneficial to operate the divertor in the so-called "snowflake-plus" mode, where the current in divertor coils is somewhat higher than the one that corresponds to exact snowflake configuration. In this case, if the configuration remains symmetric with respect to the $x$=0 plane, the expansion of the flux function near the null-point acquires the form:

$$\Phi = \frac{I}{c}\left[\mu_1 z + \mu_2 \frac{x^2 - z^2}{2} + (A + \mu_3)\left(x^2 z - \frac{z^3}{3}\right)\right] + C, \tag{4}$$

where $\mu_1$, $\mu_2$ and $\mu_3$ are proportional to

$$\varepsilon \equiv \frac{I_d - I_{d0}}{I_{d0}}. \tag{5}$$

The constant $C$ is determined by the condition that the poloidal magnetic flux be zero ($\Phi$=0) on the separatrix. In the exact snowflake configuration described by Eq. (2) this constant is zero.

In the reference case of Fig. 1, $\mu_1 = 2\varepsilon/a$, $\mu_2 = 2\varepsilon/a^2$, $\mu_3$= and the whole expansion acquires the form

$$\Phi = \frac{2I}{c}\left[\varepsilon\frac{z}{a} - \varepsilon\frac{x^2 - z^2}{2a^2} + \left(\varepsilon + \frac{a+b}{2a^2b^2}\right)\left(x^2 z - \frac{z^3}{3}\right)\right] + C. \tag{6}$$

As this expansion is to be applied in the vicinity of the magnetic field null, $x$ and $z$ in (6) are much smaller than $a$ and $b$, i.e. $x/b<<1$, $z/b<<1$. Therefore, among the contributions containing ε, the first term is dominant. One can, therefore, use, instead of Eq. (6), a somewhat simplified expansion:

$$\Phi = \frac{2I}{c}\left[\varepsilon\frac{z}{a} + \frac{a+b}{2a^2b^2}\left(x^2 z - \frac{z^3}{3}\right)\right] + C \tag{7}$$

Likewise, one can neglect terms containing $\mu_2$ and $\mu_3$ in Eq. (4). The neglected terms are of order of $\varepsilon^{1/2}$ and higher than the retained ones. An expression for $C$ will be presented shortly.

The components of the poloidal magnetic field, according to Eqs. (1) and (7), are:

$$B_x = B^*\left[-\varepsilon + \frac{a+b}{2ab^2}\left(z^2 - x^2\right)\right], \tag{8}$$

$$B_z = B^*\frac{a+b}{ab^2}xz, \tag{9}$$

where

$$B^* \equiv \frac{2I}{ac}. \tag{10}$$

Eqs. (8) and (9) show that, at $\varepsilon > 0$, there are two null-points near the origin:

$$x = 0, \quad \frac{z}{a} = \pm\sqrt{\nu} \tag{11}$$

where

$$\nu = \varepsilon\frac{2b^2}{a(a+b)} \tag{12}$$

One of the null-points lies above the x-axis, and the other below. The first one lies on the separatrix surrounding the core plasma, whereas the second one lies in the private flux region and is of lesser importance for the purpose of this discussion.

Substituting $x = 0,\ \ z/a = \sqrt{\nu}$ into Eq. (7) and imposing condition that $\Phi$ at this point is equal to zero, we find the constant $C$:

$$C = -\frac{2I}{c}\frac{a(a+b)}{3b^2}\nu^{3/2} \tag{13}$$

Using this expression and definition (12), one can present the flux as

$$\Phi(x,z) = B * \frac{a^2(a+b)}{b^2}\left(\nu\frac{z}{a} + \frac{x^2 z - z^3/3}{a^3} - \frac{2}{3}\nu^{3/2}\right) \tag{14}$$

The global structure of the separatrix in a snowflake-plus case is illustrated by Fig. 3. We present there also the separatrix for a snowflake-minus case. In this latter case, two nulls are formed on the separatrix, with a small distance between them. Here a linear contact between the plasma core and what may be called a private flux region is formed. This configuration is in many respects significantly different from the snowflake-plus configuration. We will not discuss its properties in this paper.

To compare various geometrical parameters in the case of a snowflake or snowflake-plus configuration with similar parameters for the "standard" X-point geometry, we consider as a reference for the latter a two-wire model, which reproduces some generic X-point geometry (Fig. 2). In order the magnetic field null to be in the origin, the current in the divertor coil should be equal to $I(b_1/a)$, where $b_1$ is the distance between null and the divertor conductor (shown as a light lower circle in Fig.2). We use subscript "1" for $b_1$ to avoid confusion with the snow-flake notation. For this configuration, the flux near the X-point can be presented as

$$\Phi = B * \frac{x^2 - z^2}{2a}\left(1 + \frac{a}{b_1}\right) \tag{15}$$

Note that, for $b_1 \approx 2b$, the main part of the separatrix in this X-point configuration does not differ too much compared to the reference snowflake geometry. The components of the poloidal magnetic field in this case are:

$$B_x = B * \frac{z}{a}\left(1 + \frac{a}{b_1}\right) \tag{16}$$

$$B_z = B * \frac{x}{a}\left(1 + \frac{a}{b_1}\right) \tag{17}$$

As has already been mentioned, for a pure snowflake ($\varepsilon$=0), the poloidal field scales as a square of the distance from the null-point,

$$B_P \equiv \sqrt{B_x^2 + B_z^2} = B * \frac{a(a+b)}{2b^2}\frac{r^2}{a^2} \tag{18}$$

For the standard X-point configuration $B_P$ scales linearly with $r$,

$$B_P = B * \frac{a + b_1}{b_1}\frac{r}{a} \tag{19}$$

In the case of a snowflake-plus configuration, in the immediate vicinity of the null, the magnetic field varies linearly with the distance from the null, with the gradient proportional to

$$\left|\nabla B_P\right|_{x=0,z=a\sqrt{\nu}} = \frac{B^*}{a}\sqrt{\nu} \tag{20}$$

At larger distances from the null, the quadratic dependence takes over. At these larger distances the properties of the magnetic field do not differ significantly from those of an exact snowflake. So, despite the fact that we consider a snowflake-plus configuration, in a number of cases where one does not need to consider the field geometry in a very close proximity to the separatrix, we use the field representation for an exact snowflake, $\varepsilon$=0. Only in a few cases where retaining small terms is important (e.g., evaluating shear near the separatrix) we consider the effect of a finite $\varepsilon$.

## III. FLUX SURFACES ADJACENT TO THE SEPARATRIX

The divertor operation depends on the plasma properties on the flux surfaces adjacent to the separatrix. The poloidal magnetic flux threading the layer between the separatrix and an adjacent flux surface is constant and can be expressed in terms of its value in the equatorial plane. By the latter we mean the plane where the poloidal field is parallel to the major (vertical in our figures) axis. The location of this plane is marked by arrows in Fig. 2. We call the distance of the separatrix in this plane to the y-axis as equatorial minor radius and use a notation $r_e$. The geometrical parameters for the reference cases are summarized in TABLE 1. All of them are normalized to the distance $a$ in a pure snowflake.

Table 1. Geometrical parameters in reference cases.

| Parameter | $a$ | $b$ | $r_e$ |
|---|---|---|---|
| Snowflake geometry | 1 | b=0.3 | 0.43 |
| X-point geometry | 0.925 | $b_1$= 0.6 | 0.5 |

In our reference model of a "straight" tokamak, the major radius R is assumed to be onstant. It then drops from the condition of a constancy of the poloidal flux between the separatrix and the adjacent flux surface. Equation of this surface is simply

$$\Phi(x,z) = \delta\Phi, \tag{21}$$

with δΦ constant. Its value (per unit length along the tokamak magnetic axis) is

$$\delta\Phi = B_{pe}\Delta_e, \tag{22}$$

where $\Delta_e$ is the distance between the separatrix and chosen flux surface in the equatorial plane, and  is the poloidal magnetic field at this point. Due to the narrowness of the zone that we are interested in, one can neglect the radial variation of the poloidal field. One can check that, for our reference cases illustrated by Fig. 2, this field can be approximated, to an accuracy of better than 10%, as

$$B_{Pe} \approx \frac{2I}{r_e c} \tag{23}$$

where $r_e$ is the equatorial minor radius introduced at the beginning of this section. As we are interested in the effects which manifest themselves at the level significantly larger than 10%, we will use Eq. (23) below without further remarks.

For the analysis of Secs. V and VI, we will need an explicit expression for the x(z) dependence on a given flux surface. It can be easily obtained from Eqs. (14) and (21)-(23):

$$x^2(z) = \frac{1}{z}\left[\frac{z^3}{3} - \nu a^2 z + \frac{2}{3}a^3\nu^{3/2} + \frac{2a^2b^2}{(a+b)}\frac{\Delta_e}{r_e}\right] \tag{24}$$

The distance $\Delta_e$ is positive for the surfaces outside the separatrix and negative inside the separatrix. The equatorial thickness of the scrape-off-layer is typically in the range of 0.5-2 cm, whereas the pedestal width (inside the separatrix) is only a couple of times larger [12], so that the ratio $\Delta_e/r_e$ of interest for the divertor performance is quite small, of order of 0.01.

## IV. FLARING OF THE POLOIDAL FLUX

The distance between some magnetic surface and the separatrix near the magnetic field null increases significantly compared to that distance in the equatorial plane of the device. One of the characteristics of the flaring of the magnetic field is the minimum distance between the null-point and a magnetic surface, $\Delta_0$ (Fig. 4), in relation to the distance $\Delta_e$ between this flux surface and the separatrix near the equatorial plane. The larger the ratio

$$F \equiv \frac{\Delta_0}{\Delta_e}, \tag{25}$$

the stronger the flaring. The knowledge of flaring is important, in particular, in the issue of the penetration of neutrals into SOL near the null point.

The parameter $F$ depends significantly on the distance $\Delta_e$ and increases with decreasing $\Delta_e$ (see below). We are interested in the distances of order of a characteristic width of the scrape-off-layer (SOL) in the equatorial plane. As $\Delta_e$ is small compared to the plasma size, this flux is also small compared to the total toroidal flux. So, when the flux-surface is traced to the vicinity of the null-point, one can use expansions (4) or (7).

As an example, we find the field flaring for the snowflake divertor described by Eq. (7) with $\varepsilon$=0. As is clear from the symmetry arguments, the minimum distance from the flux-surface and the null-point lies in this case on the line forming an angle of 30 degrees with the $x$ axis, so that the coordinates of the point of the minimum distance are

$$x_0 = \Delta_0\sqrt{3}/2, \quad z_0 = \Delta_0/2. \tag{26}$$

Substituting this expression to Eq. (7) with $e$=0 and using Eqs. (19) and (20), one finds:

$$\Delta_0 = \left[\frac{3cB_{Pe}a^2b^2\Delta_e}{I(a+b)}\right]^{1/3} \tag{27}$$

The flux expansion parameter $F$ (Eq. (25)) is then

$$F_S = \left[ \frac{3cB_{Pe}a^2b^2}{I\Delta_e^2(a+b)} \right]^{1/3}, \tag{28}$$

where the subscript "S" refers to a snowflake divertor. Similarly, for the reference model of the standard X-point, the minimum distance lies on the $x$ axis ( $x_0 = \Delta_0$, $z_0$=0); using Eqs. (15) and (21), (22), one finds the flux expansion parameter:

$$F_X = \left[ \frac{cB_{pe}a^2b_1}{I\Delta_e(a+b_1)} \right]^{1/2} \tag{29}$$

One can further simplify Eqs. (28) and (29) by using Eq. (21). Now only geometrical parameters of the system enter the answer:

$$F_S = \left( \frac{r_e}{\Delta_e} \right)^{2/3} \left[ \frac{6a^2b^2}{r_e^3(a+b)} \right]^{1/3} \tag{30}$$

$$F_X = \left( \frac{r_e}{\Delta_e} \right)^{1/2} \left[ \frac{2a^2b_1}{r_e^2(a+b_1)} \right]^{1/2} \tag{31}$$

The coefficient in the square bracket is of order one in both cases. The main difference is in the stronger dependence of the flux expansion over the distance from the separatrix in the snowflake case. As the ratio $r_e/\Delta_e$ is quite large, being ~100 even at the outer boundary of the scrape-off layer, the expansion is noticeably stronger in the snowflake case (by a factor of 1.5-3 for the typical scrape-off layer). This is illustrated by Fig. 5.

Another way of characterizing the flux expansion is comparing the minimum of the poloidal magnetic field on a certain flux surface, $B_{min}$, to the value of the poloidal field in the equatorial plane, $B_e$. We denote the corresponding ratio by $G$, $G \equiv B_e / B_{\min}$. In the snowflake case with $\varepsilon$=0, the magnetic field strength in the vicinity of the null-point is determined by Eq. (18), with $r=\Delta_0$. Repeating the derivation that led us to Eq. (30), we find:

$$G_S = \left( \frac{r_e}{\Delta_e} \right)^{2/3} \left[ \frac{2a^2b^2}{9r_e^3(a+b)} \right]^{1/3} \tag{32}$$

In a very similar fashion, one can show that for our reference X-point configuration the analogous parameter is

$$G_X = \left( \frac{r_e}{\Delta_e} \right)^{1/2} \left[ \frac{a^2b_1}{2r_e^2(a+b_1)} \right]^{1/2} \tag{33}$$

These parameters are also plotted in Fig. 5.

The corresponding results for the snowflake-plus configuration are illustrated by Fig. 6. When we switch from the exact snowflake to the snowflake-plus configuration, the parameter $F_s$ somewhat decreases. Its dependence on the parameter $\varepsilon$ is shown in Fig. 6 for two values of the parameter $r_e/\Delta_e$. The value $\varepsilon$=0 corresponds to an exact snowflake. One sees that the decrease is modest for $\varepsilon$ <0.05. For reference purpose, the parameter $F_X$ for the same two values of $r_e/\Delta_e$ is shown as two horizontal lines.

## V. THE CONNECTION LENGTH

An important geometrical characteristic of the divertor magnetic field is the connection length $L$ between the vicinity of the null point and the equatorial plane of the tokamak. This parameter determines the residence time of the plasma in the SOL and, therefore, may affect the SOL thickness and amount of radiative losses.

To be specific, we define it as a field line length between the equatorial plane and the poloidal magnetic field minimum. The arc segment of the field line, $dl$, is related to the segment in the poloidal projection, $ds$, by

$$dl = \frac{B}{B_P} ds \tag{34}$$

As the poloidal magnetic field becomes small in the vicinity of the null-point, the main contribution to the integral over $ds$, that determines $L$, comes from the vicinity of the null-point. This means that the total magnetic field in the numerator can be approximately replaced by the toroidal magnetic field $B_T$ in the vicinity of the null-point. Using also an identity $ds/B_P = dz/B_z$, one can present the following approximate expression for the connection length $L$:

$$L \approx B_T \int_{z_{\min}}^{z_{\max}} \frac{dz}{B_z} \tag{35}$$

The lower integration limit is the coordinate $z$ of the poloidal magnetic field minimum. With regard to the upper limit, we note that in the standard X-point divertor the connection length depends of $z_{max}$ only logarithmically. We will therefore take as an upper limit the value $z_{\max} = r_e$, corresponding, roughly, to the equatorial plane. For the snowflake divertor, the integral (35), as we will see, converges rapidly at large z, so that the choice of the upper integration limit is unimportant. Therefore, we use $z_{\max} = r_e$ in both cases.

The $z$-dependence of $B_z$ on the flux surface is determined by Eq. (9), with $x$ as in Eq. (24). For the pure snowflake divertor, one has $\nu$=0, and Eqs. (9) and (24) yield:

$$B_z = B^* \frac{a(a+b)}{b^2} \sqrt{z\left(\frac{z^3}{3} + \frac{2a^2b^2}{a+b}\frac{\Delta_e}{r_e}\right)} \tag{36}$$

In the pure snowflake case, according to Eq. (26), $z_0 = \Delta_0/2$, with $\Delta_0$ determined by Eq. (27). Then, integral (27) yields:

$$L_S = \frac{L^*}{4}\left[\frac{2b^2}{a(a+b)}\right]^{2/3} \int_0^{\infty} \frac{d\xi}{\sqrt{\xi\left(\frac{\xi^3}{3}+1\right)}} \approx 1.33 L^* \left[\frac{b^2}{a(a+b)}\right]^{2/3} \left(\frac{r_e}{\Delta_e}\right)^{1/3} \tag{37}$$

where

$$L^* \equiv \frac{B_T c a^2}{2I} = \frac{B_T a^2}{B_{Pe} r_e}. \tag{38}$$

In an analogous way, using Eqs. (15), (17) and (21)-(23) for the reference case of the standard divertor, one finds

$$L_X = \frac{L^* b_1}{2(a+b_1)} \left\{ \ln\left[\frac{2r_e^2(a+b_1)}{a^2 b_1}\right] + \ln\frac{r_e}{\Delta_e} \right\} \tag{39}$$

The comparison of the connection lengths for our two reference cases is presented in Fig. 7. One sees that the difference of the connection lengths becomes significant only quite close to the separatrix.

## VI SAFETY FACTOR AND MAGNETIC SHEAR INSIDE THE SEPARATRIX

The MHD safety factor $q$ inside the separatrix is defined in a standard way:

$$q = \frac{1}{2\pi}\oint \frac{B_T dl}{RB_P} \tag{40}$$

where $B_T$ is the toroidal magnetic field, $R$ is the major radius, and integration is carried out in the poloidal plane over a given magnetic surface. We will be interested in the safety factor near the separatrix, where the effect of the divertor magnetic field is the strongest. As has been mentioned in the previous section, the poloidal magnetic field is small near the null-point, so that the main contribution to the integral in Eq. (40) comes from the vicinity of the null-point. Taking into account this fact and using the identity $dl/B_P = dz/B_z$, one arrives at the following approximate expression for the safety factor:

$$q \approx \frac{B_T}{2\pi R} 2\int_{z_{\min}}^{r_e} \frac{dz}{B_z} \tag{41}$$

where $z_{min}$ is a coordinate of the point nearest to the null (Fig. 8); it obviously lies in the symmetry plans $x$=0, and can be found from the equation (see Eq. (24)):

$$\frac{z_{\min}^3}{3} - \nu a^2 z_{\min} + \frac{2}{3}a^3\nu^{3/2} + \frac{2a^2b^2}{(a+b)}\frac{\Delta_e}{r_e} = 0 \tag{42}$$

This $z_{min}$ should not be confused with the analogous parameter in the previous section: that one referred to the $z$-coordinate of the nearest to the null point on the flux surface outside the separatrix, Eq. (26).

As we are interested in controlling the shear effect near the separatrix by small changes of the divertor current (and, thereby, by changes of the parameters ε and ν), we retain the corresponding terms containing ν in the equations that follow. In the case of a snow-flake-plus (as well as in the pure snowflake divertor) the integral in (41) rapidly converges at the upper limit. Introducing dimensionless parameter

$$\varsigma_{\min} = \frac{z_{\min}}{a\nu}, \tag{43}$$

and using Eqs. (9), (24), (41), and (42) one arrives at the following equation for the safety factor:

$$q_S = q^* \frac{2b^2}{a(a+b)}\sqrt{\frac{3}{\nu}} I(\varsigma_{\min}) \tag{44}$$

where

$$q^* = \frac{aB_T}{2\pi RB^*}; \tag{45}$$

the dimensionless function $I(\zeta_{min})$ is defined by the equation

$$I(\varsigma_{\min}) = \int_{\varsigma_{\min}}^{\infty} \frac{d\varsigma}{\sqrt{\varsigma\left(\varsigma^3 - \varsigma_{\min}^3 - 3\varsigma + 3\varsigma_{\min}\right)}}, \tag{46}$$

with the dimensionless parameter $\zeta_{min}$ being related to the flux-surface "tag" $\Delta_e$ by:

$$\frac{\Delta_e}{r_e} = -\frac{\nu^{3/2}}{3}\frac{a(a+b)}{2b^2}\left[2+\zeta_{min}^3-3\zeta_{min}\right] \tag{47}$$

As $\Delta_e<0$ inside the separatrix, $\zeta_{min}>1$. The function $q_S(\Delta_e/r_e)$ is determined by parametric equations (46) and (47), with $\zeta_{min}$ being a parameter. Its plot is shown in Fig. 9 for several values of $\nu$.

For the standard X-point divertor described by Eqs. (13) and (17) the safety margin, as determined from Eq. (41), is:

$$q_X \approx q^*\frac{2b_1}{a+b_1}\ln\left(\frac{2r_e}{a}\sqrt{\frac{a+b_1}{2b_1}}\sqrt{\frac{r_e}{|\Delta_e|}}\right) \tag{48}$$

The corresponding curve is shown in blue in Fig. 9.

Now we switch to evaluation of the magnetic shear in the vicinity of the separatrix. We define it as

$$S=r_e dq/d\Delta_e. \tag{49}$$

For the X-point divertor, we find from Eq. (48):

$$S_X \equiv q^*\frac{b_1}{a+b_1}\frac{r_e}{|\Delta_e|} \tag{50}$$

For the snowflake-plus divertor, one can present it as:

$$S_S = q^*\frac{2b^2 r_e}{a(a+b)}\sqrt{\frac{3}{\nu}}\frac{dI(\zeta_{min})}{d\zeta_{min}}\frac{d\zeta_{min}}{d\Delta_e} \tag{51}$$

The right hand side can be presented as a function of by using Eq. (47). The resulting dependence is illustrated by Fig. 10.

## VII. GEOMETRY OF FLUX TUBES IN THE OPEN FIELD LINE REGION

In the open field line region, the plasma pressure is typically small, and plasma dynamics is determined by flute-like structures aligned with magnetic field lines. In particular, filamentary structures (sometimes called "blobs", [17]) are often present [18]. The dynamics of such structures is significantly affected by the presence of a magnetic field null and associated squeezing of the flux-tubes [11, 15, 19]. In this section we describe squeezing for the snowflake geometry and find that it is much stronger than in the case of a standard X-point divertor. Later in the section, we consider also transformations of flux-tubes associated with flute-like displacements.

Consider a fluxtube whose cross-section is circular at some point above the null-point (Fig. 11a). When one follows this fluxtube towards the vicinity of the null point and further to the divertor region, one finds that the cross-section is squeezed and becomes elliptic, very much like in the case of a standard X-point divertor [11]. We denote the minor and major semi-axes of the fluxtube cross-section as $w_{major}$ and $w_{minor}$. It is assumed that the cross-section is small enough, so that $w_{major}$ doesn't anywhere exceed the length-scale of the magnetic field. As the flux through the cross-section remains the same along the length of the flux-tube, and the field strength doesn't vary significantly, this means that the product of the semi-axes remains constant, so that $w_{minor}w_{major} = w_0^2$. One can conveniently characterize this stretching-squeezing effect by the parameter called "elongation", the ratio of the long semi-axis to the initial radius,

$$E = \frac{w_{major}}{w_0} > 1 \tag{52}$$

Obviously, $w_{minor} = w_0 / E$. The elongation, as well as orientation of the axes of the ellipse, depend on the position along the flux-tube. The situation is illustrated by Fig. 11, where both snowflake and "standard" geometry are shown.

Equations describing the elongation for the snowflake are derived in Appendix II. For the fluxtube starting as a circular fluxtube at the point "0", the elongation at the point "1" (the closest approach to the null) is

$$E_{1S} \approx 0.62 \frac{l_1^3}{\Delta_{0S}^3} \tag{53}$$

where $l_1$ is the distance along the separatrix from the magnetic null to the point "0" Fig. 11), and it is assumed that $l_1$ exceeds $\Delta_{0S}$ at least by a factor of 2. The ellipse is tilted by an angle of approximately 40 degrees with respect to the flux surface. If we continue to follow the fluxtube further to the divertor region (point 2), we find that the ellipse gets aligned with the flux surface, and the elongation becomes

$$E_{2S} \approx 0.38 \frac{l_1^3 l_2^3}{\Delta_{0S}^6} \tag{54}$$

Where it is assumed that $l_2$ is greater than $\Delta_{0S}$.

For comparison, in the case of the standard X-point, the elongation at point 1 is (Cf. Ref. [FPR])

$$E_{1X} = \frac{l_1}{\sqrt{2}\Delta_{0X}}, \tag{55}$$

And elongation at point "2" is

$$E_{2X} = \frac{l_1 l_2}{\sqrt{2}\Delta_{0X}}. \tag{56}$$

Unlike the snowflake case, the major axis of the ellipse does not rotate and remains aligned with one of the branches of the separatrix (Fig. 11b).

The stretching/squeezing in the case of the snowflake divertor is significantly stronger than for the standard divertor. This observation is important in the context of the flute-like modes in the SOL [20-22]. For example, strong stretching/squeezing may make the thickness of the initially thick fluxtube smaller than the ion gyroradius [11, 23], thereby making purely MHD flute-like modes impossible. Likewise, in the analysis of the dynamics of blobs, strong squeezing may cause disconnection of the blob from the divertor plates [15, 24]. For the snowflake configuration these effects are significantly stronger.

Consider now displacements of the center line of the fluxtube driven by the normal displacement of its end (point "0") in Fig. 12. This kind of transformations is important, in particular, in the analysis of the blob dynamics: The only allowed motion of the low-beta, high-conductivity plasma filling a flux-tube is the one that maps the initial flux tube into another flux tube (a flute-type displacement). For example, the normal displacement of a point "0" leads to both normal and poloidal displacements of any Lagrangian point on the flux-tube. Expressions for such transformations in a general geometry are presented in Ref. [25]. Here we present these expressions for points "1" and "2" on Fig. 12 .

At point "1" both tangential and normal displacements are present:

$$u_{1nS} \approx 0.6E_{1S}u_{0n}, \;\; u_{1tS} \approx 0.8E_{1S}u_{0n}, \tag{57}$$

whereas at point "2", the tangential component becomes completely dominant:

$$u_{2tS} \approx 0.8E_{2S}u_{0n}; \;\; u_{2nS} << u_{2tS} \tag{58}$$

For the standard divertor these displacements are much smaller.

## VIII. SENSITIVITY TO VARIATIONS OF THE PLASMA CURRENT

In Ref. [6] it was shown that the snowflake-plus configuration is quite robust to possible variations of the plasma current: the change of the plasma current by ± 2 % does not change the configuration in a significant way. Here we consider possible effect of lateral displacements of the plasma current. To imitate this effect, we assume that the central conductor (imitating the plasma current in our reference model) is displaced along the axis x by the distance of ± $0.02r_e$. The results are shown in Fig. 13 . We see that lateral displacements also produce a relatively minor effect on the snowflake-plus configuration.

## IX. SUMMARY AND DISCUSSION

In this paper, we provided a detailed characterization of the geometrical properties of a snowflake divertor which, on one hand, may serve as input parameters for the analysis of various plasma effects in the snowflake geometry and, on the other hand, can serve as a guidance in more detailed design studies of such divertors. In order to more clearly reveal the differences from the standard X-point divertor we presented the corresponding results for this configuration as well.

The set of coils required to generate the snowflake configuration is quite simple, and the divertor coil current is in the range of 50% of the plasma current per coil. The distance from the coils to the magnetic null is large, thereby allowing for placing the coils outside toroidal field coils.

The snowflake-plus configuration is quite robust with respect to possible uncontrolled variations of the plasma current. It does not impose too severe constraints on the poloidal feedback system (1-2% deviations from the "dialed in" currents in the poloidal field coils lead to only minor changes of the configuration).

In addition to an obvious effect on the flux expansion near the null point (typically, by a factor of 2 compared to the X-point configuration), the snowflake divertor provides additional degree of control over a variety of processes in the scrape-off-layer and in the pedestal region. It allows one to control the magnetic shear in the pedestal region just inside the separatrix, thereby providing a tool for affecting the ELM activity. It leads to a stronger squeezing of the magnetic flux-tubes passing near the magnetic null point, thereby affecting the divertor-leg instabilities and instabilities in the vicinity of the null-point. Isolated fluxtubes (blobs) manifest much faster motions in the vicinity of the null point than their counterparts in a standard configuration, for the same radial velocity in the equatorial plane. This leads to an increased inertia of the blobs. Large poloidal displacements of the ends of the blob significantly enhance the effect of the boundary conditions on the divertor plates.

**ACKNOWLEDGMENT**

This work was performed under the auspices of the U.S. Department of Energy by Lawrence Livermore National Laboratory under Contract DE-AC52-07NA27344.

## APPENDIX A: THE PROPERTIES OF THE FUNCTION I, EQ. ()

The function $I(\zeta_{min})$ is shown in Fig. 14. Consider asymtotics of the function I for $\zeta_{min}-1<<1$ and $\zeta_{min}-1>>1$. The condition $\zeta_{min}-1<<1$ corresponds to the flux surfaces lying very close to the separatrix, so that they "probe" the zone where the linear dependence of the magnetic field holds ($\Delta_0/a < \sqrt{\nu}$, see Sec.II). Here the dependence of $I$ on $\zeta_{min}$ is logarithmic,

$$I(\zeta_{\min}) \approx \frac{1}{\sqrt{3}} \ln \frac{3.1}{\zeta_{\min}-1}, \quad \zeta_{\min}-1 << 1. \tag{A.1}$$

At large $\zeta_{min}$ the flux surfaces stay in the area where the quadratic (snowflake) dependence of the magnetic field is dominant. Here $I$ scales as $1.4/\zeta_{min}$ :

$$I(\zeta_{\min}) \approx \frac{1.4}{\zeta_{\min}}, \quad \zeta_{\min}-1 >> 1 \tag{A.2}$$

Note that large $\zeta_{min}$ are still compatible with small $\Delta_e$, because of the presence of the factor $\nu^{3/2}$ in the r.h.s. of Eq. (47). One should, however, remember that in all our analysis we use an assumption $\Delta_e/r_e<<1$.

There is a convenient interpolation between the two limits (A.1) and (A.2):

$$I(\zeta_{\min}) \approx \frac{1}{\sqrt{3}} \ln \sqrt{\frac{3.1^2}{(\zeta_{\min}-1)^2}+1} + \frac{1.4\zeta_{\min}}{4+\zeta_{\min}^2}. \tag{A.3}$$

It has an accuracy of better than a few percent in the whole domain $1< \zeta_{min} <\infty$.

In the calculation of the magnetic shear, one uses Eq. (47), which yields:

$$\frac{d\Delta_e}{d\zeta_{\min}} = -\frac{\nu^{3/2} a(a+b)}{2b^2}\left(\zeta_{\min}^2-1\right) \tag{A.4}$$

Eqs. (51) and (A.3) then yield:

$$S_S = q * \frac{\sqrt{3}}{\nu^2\left(\zeta_{\min}^2-1\right)}\left[-\frac{1}{\sqrt{3}}\frac{3.1^2}{(\zeta_{\min}-1)\left[3.1^2(\zeta_{\min}-1)^2+1\right]} + \frac{1.4(4-\zeta_{\min}^2)}{(4+\zeta_{\min}^2)^2}\right], \tag{A.5}$$

with the dependence $\zeta_{min}(\Delta_e/r_e)$ determined implicitly by Eq. (47). As $\Delta_e<0$ inside the separatrix, $\zeta_{min}>1$.

## APPENDIX B: SQUEEZING OF THE FLUX TUBES IN THE SCRAPE-OFF-LAYER

Here we consider a pure snowflake divertor. In this case, the magnetic field structure in all 6 sectors is identical. It is convenient to consider the structure in the sector pointing upwards. There is a direct correspondence between each point in this sector and the sector of the common flux outside the separatrix Fig. … a, to which we will eventually apply our results.

Consider an initial point with coordinates $X_0$, $Z_0$ (Fig. 11a). This point situated in some toroidal location determines the whole field line. This will be a center line of the flux tube. In some other poloidal cross-section this field line will come to the closest distance to the null-point, i.e., to the point "1" in Fig. 15. Its coordinates will be $Z_1=\Delta_0$,

$X_1$=0. If we move further along the field line, we reach the point with some coordinate $Z_2$, $X_2$. The whole field line is defined by the equation

$$X^2 Z - \frac{Z^3}{3} = -\frac{\Delta_0^3}{3} \tag{B.1}$$

Below, we assume that the points "0" and "2" are situated at the distance a few times greater than $\Delta_0$ along the separatrix.

We use two approximations which hold quite well in the vicinity of the null-point. First, we consider the toroidal magnetic field as uniform; second, we assume that it is much higher than the poloidal field. This latter assumption means that the normal cross-section of the flux tube is the same as the cross-section by the poloidal plane. The fact that the toroidal field is uniform, allows one to say that the distance between two poloidal cross-sections along the field line is just $B_T \int \frac{dz}{B_z}$, where integration is performed between these two points.

Consider now points that are situated in the vicinity of the initial point, $X_0 + \xi_0, Z_0 + \varsigma_0$. To find the parameter called "elongation", one has to assume that lie on the circle of some infinitesimal radius with the center on the central field line. The mapping of this point to the cross-section, where the central field lines reaches its closest approach to the null-point, is determined by the equations (Cf. Sec. V):

$$\int_{Z_1+\varsigma_1}^{Z_0+\varsigma_0} \frac{dz'}{\sqrt{z'\left[z'^3 - \left(Z_1+\varsigma_1\right)^3 + 3\xi_1^2(Z_1+\varsigma_1)\right]}} = \int_{Z_1}^{Z_0} \frac{dz'}{\sqrt{z'(z'^3 - Z_1^3)}} \tag{B.2}$$

and

$$2X_0 Z_0 \xi_0 + \left(X_0^2 - Z_0^2\right)\varsigma_0 = -Z_1^2 \varsigma_1. \tag{B.3}$$

In the first of these equations, one has to make an expansion in the l.h.s. up to terms linear in $\xi_0, \varsigma_0$. This task is significantly simplified if the distance of the point "0" from the origin exceeds by a factor of 2 or so the distance $\Delta_0$. In this case, using $Z_1/Z_0$ as a small parameter, one finds:

$$\begin{aligned} \xi_0 &= \frac{2}{\sqrt{3}}\frac{Z_0^2}{Z_1^2}\left(\frac{2}{\sqrt{3}}\xi_0 - 1.4\varsigma_0\right) + \frac{\sqrt{3}}{2}\frac{Z_1^2}{Z_0^2}\varsigma_0; \\ \varsigma_0 &= \frac{Z_0^2}{Z_1^2}\left(\frac{2}{\sqrt{3}}\xi_0 - 1.4\varsigma_0\right) \end{aligned} \tag{B.4}$$

As it should be, the determinant of this transformation is equal to 1. This transformation immediately yields Eqs. (53) and (57). To obtain Eqs. (54) and (58), one has to use the transformation twice.

## References


1. M. Kotschenreuther, P.M. Valanju, S.M. Mahajan, J.C. Wiley. Phys. Plasmas, 14, 072502, 2007.

2. F. Najmabadi and the ARIES team, Fus. Eng. Des., **38**, 3 (1997).

3. R. Majeski, S. Jardin, R. Kaita, T. Gray, P. Marfuta, J. Spaleta, J. Timberlake, L. Zakharov, G. Antar, R. Doerner, S. Luckhardt, R. Seraydarian, V. Soukhanovskii, R. Maingi, M. Finkenthal, D. Stutman, D. Rodgers and S. Angelini. Nucl. Fusion 45 519-523, 2005

4. H. W. Kugel, M. G. Bell, J.-W. Ahn, J. P. Allain, R. Bell, J. Boedo, C. Bush, D. Gates, T. Gray,1 S. Kaye, R. Kaita, B. LeBlanc, R. Maingi, R. Majeski, D. Mansfield, J. Menard, D. Mueller, M. Ono, S. Paul, R. Raman, A. L. Roquemore, P. W. Ross, S. Sabbagh, H. Schneider, C. H. Skinner, V. Soukhanovskii, T. Stevenson, J. Timberlake, W. R. Wampler, and L. Zakharov, Phys. Plasmas 15, 056118 (2008)

5. M. Kotschenreuther et al, 2004 IAEA Fusion Energy Conference (Vilamoura, Portugal, 1-6 November 2004) paper IC/P6-43, Vienna, International Atomic Energy Agency.

6. D.D. Ryutov. 'Geometrical Properties of a "Snowflake" Divertor.' Phys. Plasmas, **14**, 064502, June 2007, UCRL-JRNL-227872; D.D. Ryutov. Phys Plasmas, **15**, #6, 2008

7. D.D. Ryutov. "A snowflake divertor and its properties". Paper D1.002, 34th EPS Conf. on Plasma Phys, Warsaw, July 2-6, 2007 (http://epsppd.epfl.ch/Warsaw/start.htm)

8. M. Kotschenreuther, P.M. Valanju, S.M. Mahajan. "High Power Density Experiment (HDPX) – A Next Step Device in the Age of ITER." Paper 1C presented at the 2008 Intern. Fusion Theory Conf, Boulder, CO, March 31-April 2, 2008.

9. R.H. Cohen, D.D. Ryutov. Nucl. Fusion, **37**, 621 (1997).

10. G.F. Counsell, A. Kirk, R.H. Cohen, et al. Nucl. Fusion, **43** 1197-1203 (2003).

11. D.Farina, R.Pozzoli, D.D. Ryutov. "Effect of the magnetic field geometry on the flute-like perturbations near the divertor X-point". Nuclear Fusion, v.33, p.1315 (1993).

12. P.B. Snyder, H.R. Wilson, J.R. Ferron, L.L.Lao, et al. Phys. Plasmas, **9**, 2037 (2002)

13. A.J. Webster, C.G. Gimblett. "The Ideal Magnetohydrodynamic Peeling Mode Instability," Paper 3B03, International Sherwood Fusion Theory Conference, Boulder, CO, 31 March – 2 April 200; A.J. Webster, C.G. Gimblett. 34th EPS Conference on Plasma Phys. Warsaw, 2-6 July 2007, ECA Vol. 31F, P-4.088

14. S.I. Krasheninnikov, D.D. Ryutov, G. Yu, "Large plasma pressure perturbations and radial convective transport in a tokamak", *J. Plasma Fusion Res. (Japan),* **6,** 139-143, (2004).

15. R.H. Cohen, D.D. Ryutov, "Dynamics of an isolated blob in the presence of the X-point", *Contrib. Plasma Phys.,* **46,** 678 (2006).

16. Petrie TW, Wade MR, Brooks NH, Fenstermacher ME, Groth M, Hyatt AW, Isler RC, Lasnier CJ, Leonard AW, Mahdavi MA, Porter GD, Schaffer MJ, Watkins JG, West WP, Team D-D. Compatibility of the radiating divertor with high performance plasmas in DIII-D. [Journal Paper] Journal of Nuclear Materials, vol.363-365, 15 June 2007, pp. 416-20.

17. S.I. Krasheninnikov. Phys. Lett. **A283**, 368 (2001).

18. S.J. Zweben, R.J. Maqueda, J.L. Terry, T. Munsat, J.R. Myra, D. D'Ippolito, D.A. Russell, J.A. Krommes, B. LeBlanc, T. Stolzfus-Dueck, D.P. Stotler, K.M. Wiliams, C.E. Bush, R. Maingi, O. Grulke, S.A. Sabbagh, A.E. White. Phys. Plasmas, **13**, 056114 (2006).

19. D.D. Ryutov, R.H. Cohen. "Geometrical effects in plasma stability and dynamics of coherent structures in the divertor." Contrib. Plasma Phys., **48**, #1-3, 48-57, March 2008

20, J.R. Myra, D.A. D'Ippolito, X.Q. Xu, R.H. Cohen. Phys. Plasmas, **7**, 2290, 2000; **7**, 4622, 2000.

21. D.A. Russel, D. A. D'Ippolito, J.R. Myra, W.M. Nevins, X.Q. Xu. Phys.Rev. Lett., **93**, 265001 (2004).

22. J.R. Myra, D. D'Ippolito. Phys. Plasmas, **12**, 92511 (2005).

23. D.D. Ryutov, R.H. Cohen. Contrib. Plasma Phys. **44**, 168 (2004).

24. R.H. Cohen, B. LaBombard, L.L. LoDestro, T.D. Rognlien, D.D. Ryutov, J.L. Terry, M.V. Umansky, X.Q. Xu, S. Zweben. Nucl. Fusion, **47**, 612 (2007).

25. D.D. Ryutov. Phys. Plasmas, **13**,122307 (2006).

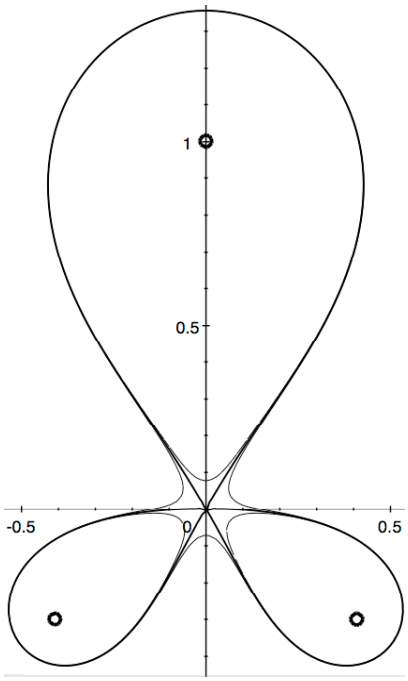


Fig. 1 Bold solid line represents a separatrix of a snowflake divertor. Thin lines represent nearby flux surfaces; their distance from the separatrix near the equatorial plane becomes too small to be distinguishable. A characteristic hexapolar structure near the field null is clearly visible. Small circles represent positions of the conductors creating this geometry. All dimensions are normalized to the distance of the main conductor from the origin.

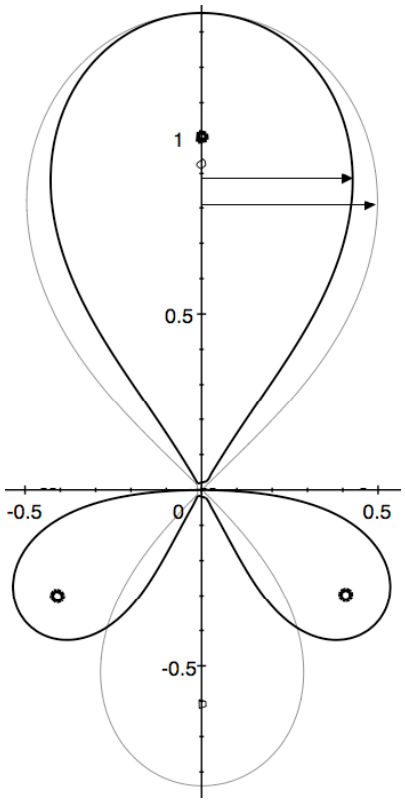


Fig. 2 A reference snowflake configuration (bold line) and reference standard X-point configuration. All the scales are normalized to the distance $a$ of the central conductor in the reference snowflake case (b=0.3$a$). Locations of two conductors in the X-point geometry are shown as light circles. Location of the main conductor in an X-point case is $z$=0.925$a$, and $b_1/a$=0.61. These parameters are chosen so as to make the distance from the null-point to the top of the separatrix the same in both cases. The equatorial radii (shown by arrows) are 0.43$a$ in the snowflake case and 0.5$a$ in the X-point case.

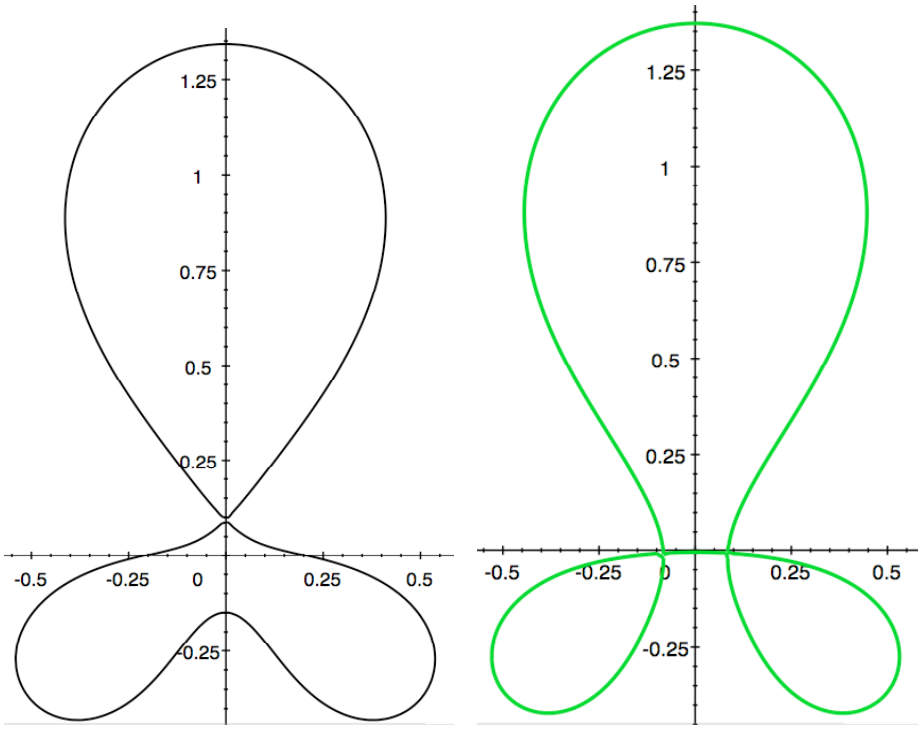


Fig. 3 Separatrixes for snowflake-plus (a) and snowflake-minus (b) configurations. The parameter $\varepsilon$ is +0.05 and -0.05, respectively. The ratio $b/a$ is 0.3.

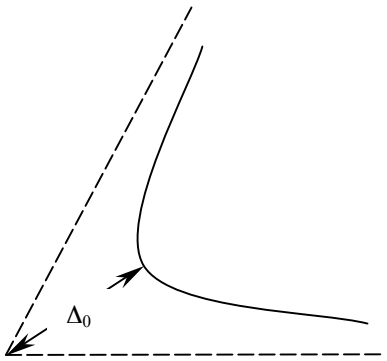


Fig. 4 Definition of the parameter $\Delta_0$: the separatrix is shown by dashed lines, whereas the adjacent flux surface by the solid line. The null-point is situated in the intersection of two branches of the separatrix.

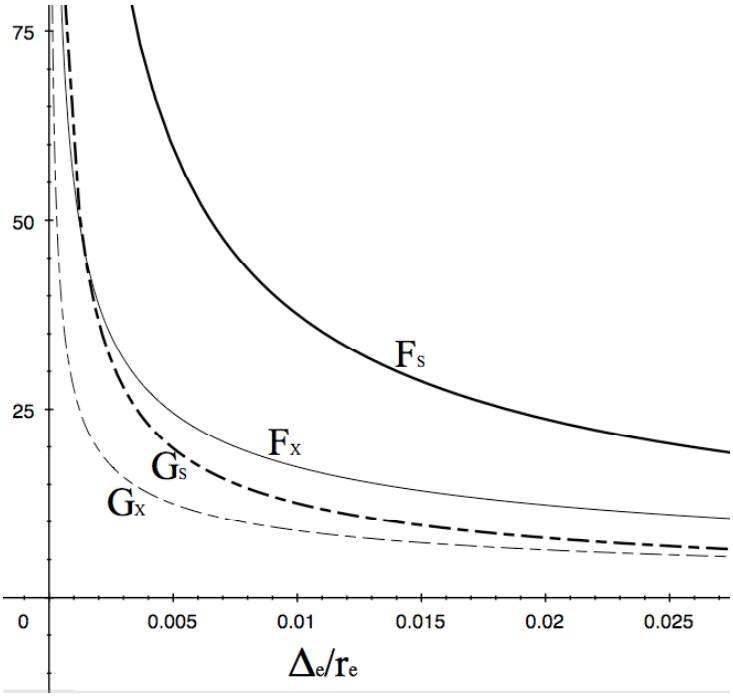


Fig. 5. Geometrical expansion parameters for a snowflake (Eq. (25), bold line) and X-point configurations (Eq. (26), thin line). "Input" parameters are taken from Table 1. For the typical SOL thickness the ratio $F_S/F_X$ is in the range of 1.5-3. Dashed lines represent the magnetic expansion parameter $G$. The ratio $G_s/G_X$ is in the range 1.2-2.

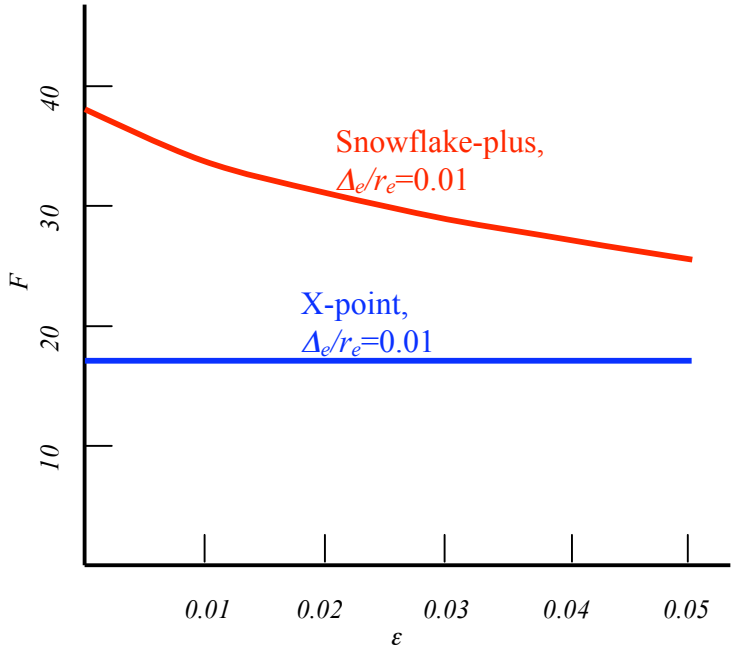


Fig. 6. Flux expansion parameter F for the snow-flake plus divertor (red curve) as a function of the divertor current excess e. The blue horizontal line represent a reference value of the flux expansion in the standard X-point divertor.

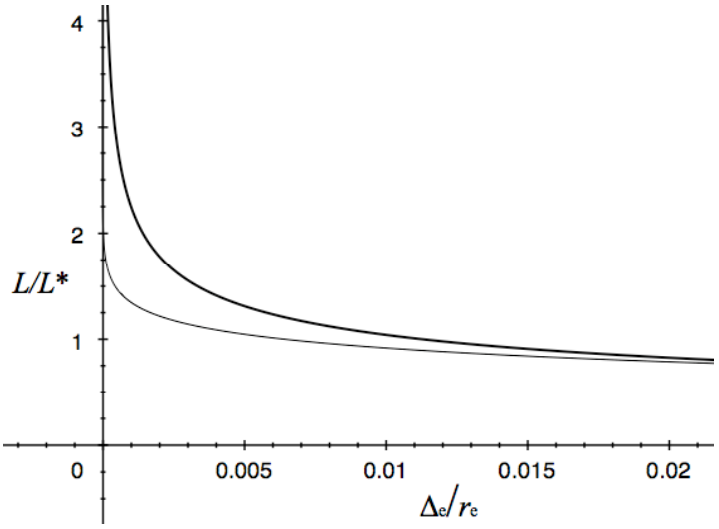


Fig. 7. Connection length for the snowflake divertor (bold line) and standard X-point divertor (light line).

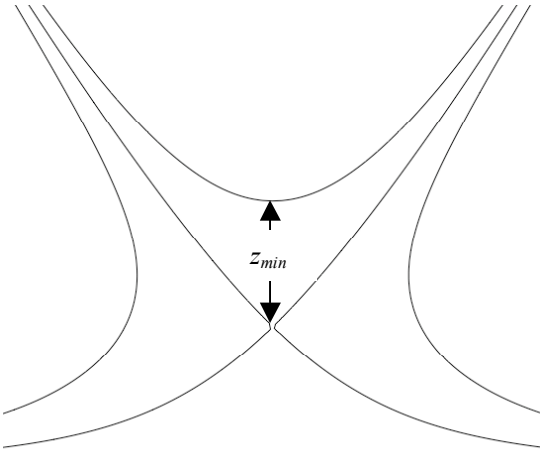


Fig. 8 Definition of $z_{min}$ for the flux surfaces inside the separatrix of a snowflake-plus divertor.

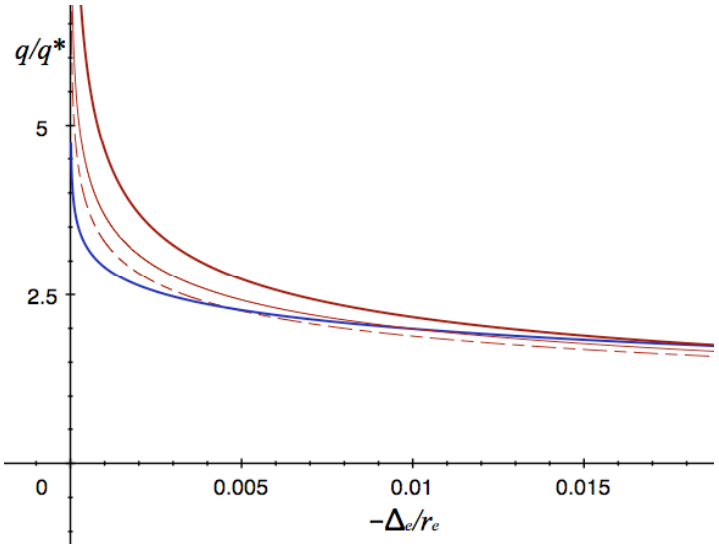


Fig. 9 Safety factor q inside the separatrix. Blue line: standard X-point divertor. Thick red line: ε=0 (pure snowflake); thin red line: ε =025; dashed red line: ε =0.05.

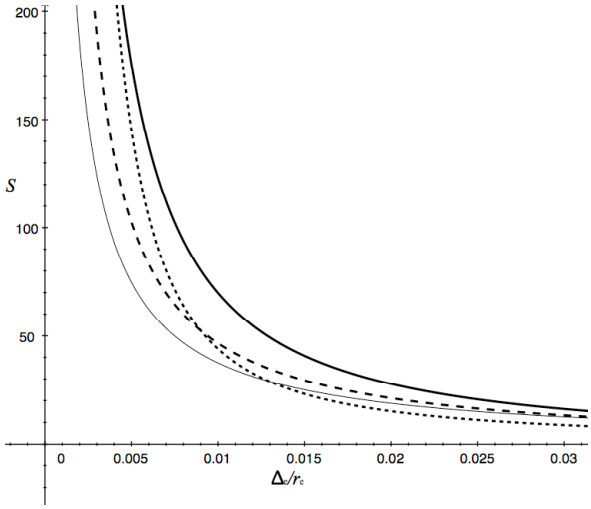


Fig. 10. Magnetic shear for the standard X-point divertor ($b_1/a$=0.6), thin line, and for the snowflake-plus divertor ($b/a$=0.3), thick lines. Solid line: $\varepsilon$=0 (an exact snowflake), $\varepsilon$=0.025 (dashed line) and ε=0.05 (dotted line). Large values of the parameter $S$ is related to the normalization. More important is the change of the $S$ profile for the snowflake divertor compared to that of a standard divertor: in the immediate vicinity of the separatrix, the snowflake-plus divertor yields higher value of $S$, whereas at some distance from the separatrix, deeper into the pedestal region, $S$ can become both larger and smaller than for the X-point divertor. This can be used to control ELM activity.

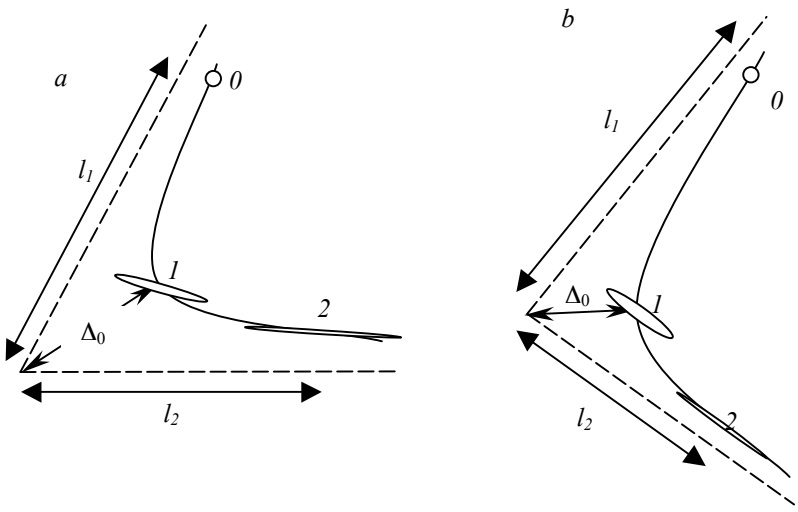


Fig. 11. Flux-tube squeezing in a snowflake divertor (a) and in a standard X-point divertor (b).

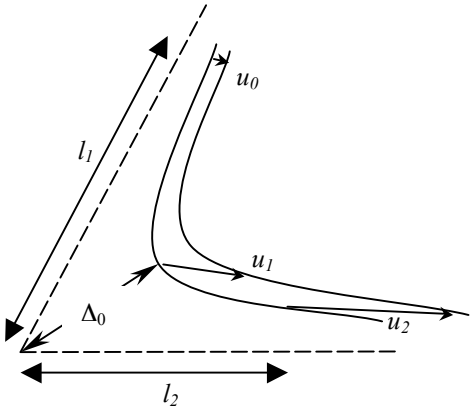


Fig. 12. Mapping of the flux tube.

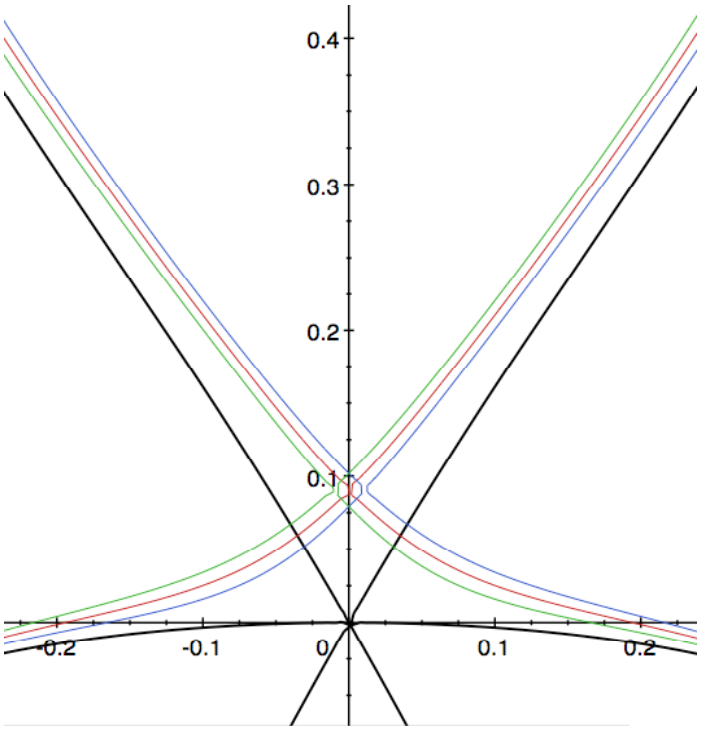


Fig. 13. The snowflake-plus configuration is insensitive to possible increases/decreases of the plasma current or its displacements

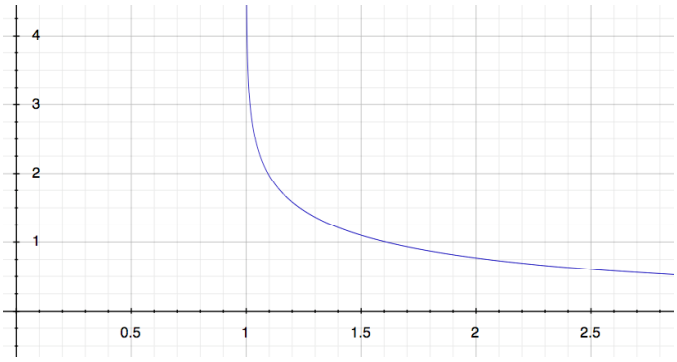


Fig. 13. Function $I(\xi_{min})$.

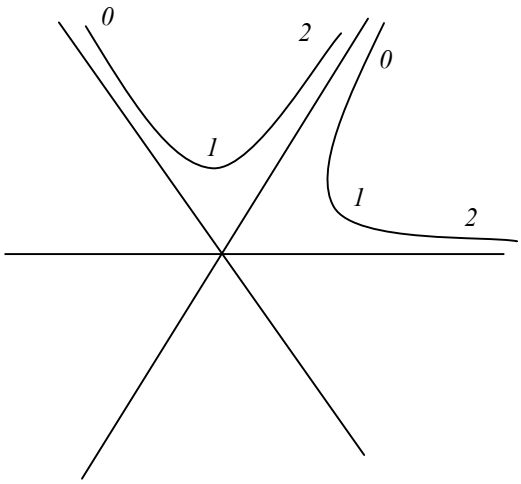


Fig. 15 Designation of the points used in the evaluation of the flux-tube mapping for a snowflake divertor